

## **CHAPTER 4**

### **TRACKING EFFICIENCY**

#### **4.1 Tracking concepts in detector**

Tracking layout of a detector typically reflects the whole view and physics purpose of the experiment. Every single part or components are constructed within the physics event required and this will mention the structure of the tracking chambers, which is known as one of the most important part of detector. In common scenarios, there are two typical concepts of tracking structure in detector, the forward or fixed-target geometry and the collider detector geometry.

##### **4.1.1 Forward or fixed-target geometry and parameters**

In the fixed-target geometry concept, the colliding or incident particle is assumed to have significantly high momentum with a huge effect of Lorentz boost. After hitting the static target in the middle of detector, emerging particles will travel forward in a cone-shaped region. To cover all possible trajectory space, in this situation, the detector layout must essentially manage to cover every single angle of the projected cone. Meanwhile, in most practice, the backward part of the solid angle is neglected and this gives the reason why this scenario is called the forward detector geometry concept.

Below are the main components of the typical forward spectrometer:

- The vertex detector, whose main purpose is to improve track detection with higher resolution near the interaction point. Reconstruction of secondary vertex or distinction of detached tracks is an important aspect of particle reconstruction in the detector.
- The spectrometer magnet and the main tracking system in forward geometry which measures momentum and determine the sign of charged particles from the curvature.
- The calorimeter system, measures the deposited shower energy from particle trajectories which then allows the identification of electrons and hadrons. The component is split into two parts, electromagnetic and hadronic. The calorimeter also measure energies of individual neutral particles, usually photons.
- The muon detector, placed at the last part of spectrometer. Muons typically having longer lifetime, are able to traverse the intermediate materials and will be detected at specific dedicated tracking layers.

The design of forward spectrometer is also influenced by the momentum resolution as at sufficiently high momentum the resolution is inversely proportional to the integral of the magnetic field along the trajectories.

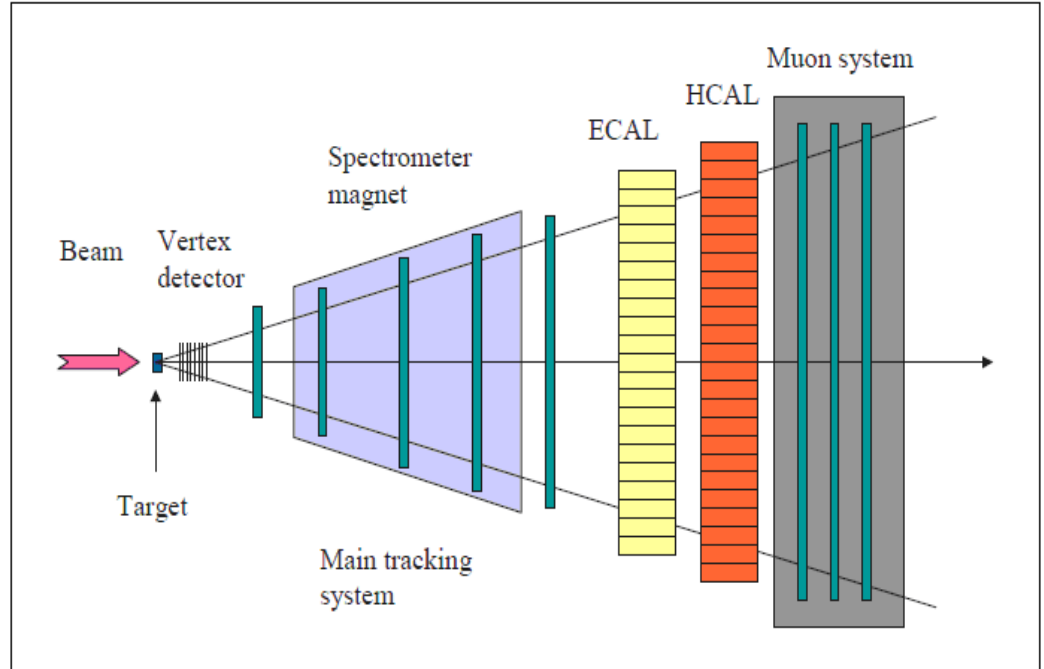


**Figure 4.1** : Typical geometry of a forward spectrometer

In the forward geometry, the interaction region lies very often in an area without magnetic field, since the spectrometer magnet is located further downstream. The natural choice of parameters, assuming that the  $z$  coordinate points down the spectrometer axis and  $x$  and  $y$  are the transverse coordinates, is then,

- $x_0$  the  $x$  coordinate at the reference  $z_0$
- $y_0$  the  $y$  coordinate at the reference  $z_0$
- $t_z = \tan \theta_x$  the track slope in the  $xz$  plane
- $t_y = \tan \theta_y$  the track slope in the  $yz$  plane
- $Q/p$  the inverse particle momentum, signed according to charge

where  $z_0$  denotes the location of a suitable reference plane transverse to the beam, for example at the position of the target, or at the nominal interaction point. The slope parameters allow for a convenient transformation of the parameters to a different reference  $z$  value, as is needed during vertex reconstruction. In cases of a very homogeneous magnetic field, it may be advantageous to substitute the parameter  $Q/p$  to  $Q/p_{\perp}$ , where  $p_{\perp}$  is the momentum in the plane transverse to the magnetic field, or by  $\kappa = Q/R$ , the signed inverse radius of the curvature.

### 4.1.2 Collider detector geometry and parameters

Collision between two particles head-on at sufficiently high momentum will require more coverage in terms of particle detection. In general, the detector needs to cover the full solid angle, which leads to a cylindrical detector layout with a solenoid field parallel to the beam axis.

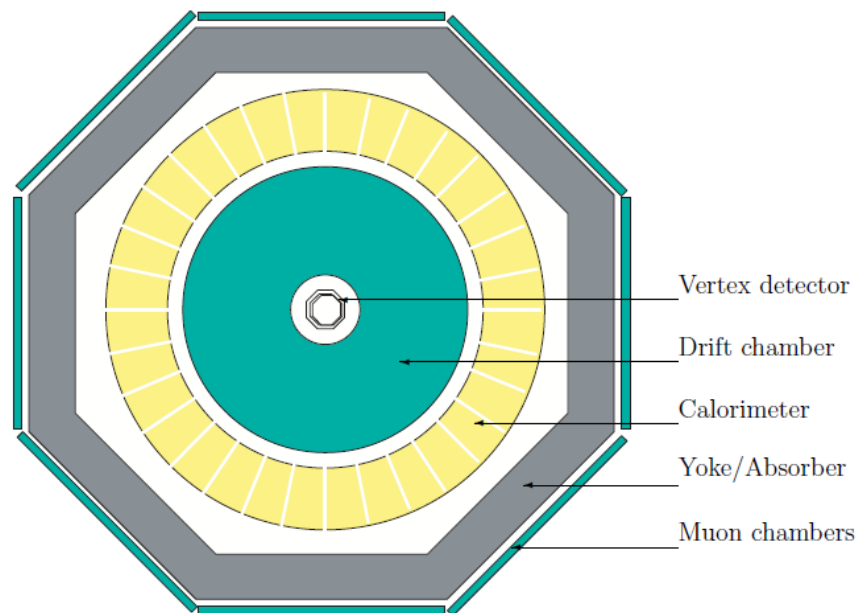


**Figure 4.2 :** Typical setup of a cylindrical or collider detector.

Somehow at some features, cylindrical geometry comes with different components structure in comparison with the forward geometry detector.

- The vertex detector located at the central part of the detector which is called the barrel part, requires modules parallel to the beam which manage to at least cover the angular acceptance near the interaction point.

- The main tracking system is located within the magnetic field; it generally consist of the coil and yoke of the magnet. The coil is preferably to be located between drift chamber and calorimeter or if possible to make it large enough to enclose the calorimeter.
- To cover full solid angle, the calorimeter will require forward, barrel and rear part.
- The muon detector, the yoke for the solenoid itself readily as absorber.

In collider detectors with cylindrical geometry, the magnetic field normally encompasses the whole tracking volume, including the interaction region where the particles are produced. In a homogeneous solenoid field, the particle trajectory will be a helix curling around an axis parallel to the magnetic field. Assuming the  $z$  coordinate is oriented along the detector axis, and the radius is given by  $r = \sqrt{x^2 + y^2}$ , typical track parameters given at a reference value  $r = r_0$  may be

- $\phi_0$  the azimuth angle where the trajectory intersects the reference radius
- $z_0$  the  $z$  value where the trajectory intersects the reference radius
- $\psi_0$  the phase angle of the helix at the reference radius intersection, which corresponds to the angle of the tangent at this point
- $Q/R$  the signed inverse curvature radius of the helix
- $\tan \lambda$  where  $\lambda = \arctan p_z / p_\perp$  is the dip angle of the helix

## 4.2 Parameter estimation

The kinematical parameters of a particle, or also referred to as track fitting parameters, are generally defined as the spatial measurements of a particle flight direction and momentum at its point of origin along the trajectories. To discuss further on this topic, two different methods will be elaborated next.

### 4.2.1 Least squares estimation

According to least squares estimation, if the trajectory of a particle can be described by a closed expression  $f_{\lambda}(\ell)$ , where  $\lambda$  stands for the set of parameters,  $\ell$  is the flight path and  $f$  is the coordinate which could be measured, a set of measurements  $\{m_i\}$  with errors  $\{\sigma_i\}$ , will provide an estimate of the parameters, giving

$$X^2 = \sum \frac{(m_i - f_{\lambda}(\ell_i))^2}{\sigma_i^2} \quad (29)$$

If the measurements  $m_i$  follow a normal distribution and the function  $f_{\lambda}$  is sufficiently linear, the expression  $X^2$  will follow a normal distribution. This property can be used for statistical test.

In the case of normally distributed measurements  $m_i$ , one can easily convince that the above impression is proportional to the negative logarithm of the corresponding likelihood function, which shows directly the equivalence of least squares principle and maximum likelihood principle for this case.

By denoting the derivative matrix for  $f$  as  $\frac{\partial f}{\partial \lambda}$ , where  $\left(\frac{\partial f}{\partial \lambda}\right)_{ij} = \frac{\partial f_{\vec{\lambda}}(\ell_i)}{\partial \lambda_j}$ , the symbolizing of this matrix with respect to the parameters as  $\mathbf{F}$  and the (diagonal) error matrix of the measurements as  $\mathbf{V} = \text{diag}\{\sigma_i^2\}$ , the expression to be minimized is

$$(\vec{m} - F\vec{\lambda})^T V^{-1}(\vec{m} - F\vec{\lambda}) \quad (30)$$

and the matrix equation

$$F^T V^{-1} \vec{f} = F^T V^{-1} \vec{m} \quad (31)$$

For linear problem  $\vec{f} = F\vec{\lambda}$ , the above condition can be directly inverted

$$\vec{\lambda} = (F^T V^{-1} F)^{-1} F^T V^{-1} \vec{m} \quad (32)$$

and the estimated parameters are a linear function of the measurements. The matrix  $(F^T V^{-1} F)^{-1}$  is inverted in the shape of  $N_\lambda \times N_\lambda$ , where  $N_\lambda$  is the number of parameters describing the particle.

Meanwhile, the covariance matrix of the parameter estimate can be directly determined as

$$\text{cov}(\vec{\lambda}) = C_\lambda = (F^T V^{-1} F)^{-1} \quad (33)$$

The least squares method is popular due to its optimality properties of linear case as follow,

- The estimate is unbiased, for instance, the expectation value of the estimate is the true value
- The estimate is efficient, whereby, of all unbiased estimates which are linear functions of the observables, this method has the smallest variance which is generally called the Gauss-Markov-Theorem.

In fact, in most cases where the function  $f_{\lambda}$  can be locally approximated by a linear expansion, these properties are still retained.

#### **4.2.2 The Kalman Filter Technique**

Different from the least squares parameter estimation which requires the global availability of all measurements at fitting time, the Kalman filter technique was developed to determine the trajectory of the state vector of a dynamical system from a set of measurements taken at different times. In considering cases such as in real-time tracking of objects, or in pattern recognition scheme which are based on track following, where it is not clear a-priori if the hit combination under consideration does really belong to an actual track, the Kalman filter technique is more convenient for estimating the measurements compared to the first method.

The Kalman filter technique efficiently improves track and vertex reconstruction based on two steps. Firstly in the prediction step, an estimate is made for the next measurement from the current knowledge of the state vector, where it is very useful to discard noise signals and hits from other tracks from the fit. Secondly in the filter step, the updates of the state vector does not require inversion of a matrix with dimension of the state vector as in a global fit, but only with the dimension of the measurement.

To describe Kalman filter in this thesis, implementation and nomenclature from [39-41] is referred. In this notation, the system state at the time, after inclusion of  $k$  measurements is denoted by  $\tilde{x}_k$ , its covariance matrix by  $C_k$ .  $\tilde{x}_k$  contains the parameters of the fitted track, given at the position of the  $k^{\text{th}}$  hit. The matrix  $F_k$  describes the propagation of the track parameters from the  $(k-1)^{\text{th}}$  to the  $k^{\text{th}}$  hit. For example, in a planar geometry with one-dimensional measurements and straight line tracks, the propagation takes the form

$$\begin{pmatrix} x \\ t_x \end{pmatrix}_k = \begin{pmatrix} 1 & z_k - z_{k-1} \\ 0 & 1 \end{pmatrix} \begin{pmatrix} x \\ t_x \end{pmatrix}_{k-1} \quad (34)$$

where a subset of the track parameterization in section 4.1.1 has been used. The coordinate measured by the  $k^{\text{th}}$  is denoted by  $m_k$ . In general  $m_k$  is a vector with the dimension of that specific measurement. For tracking devices measuring only one coordinate,  $m_k$  is an ordinary number. The measurement error is described by the covariance matrix  $V_k$ . The relation between the track parameters  $\tilde{x}_k$  and the

predicted measurement is described by the projection matrix  $H_k$ . In the example in section 4.3.2, the measured coordinate in the stereo view  $u$  is

$$H \begin{pmatrix} x \\ y \end{pmatrix} = (\cos \alpha_{st} \quad -\sin \alpha_{st}) \begin{pmatrix} x \\ y \end{pmatrix} \quad (35)$$

with  $\alpha_{st}$  as the stereo angle at  $45^\circ$ .

In each filter step, the state vector and its covariance matrix are propagated to the location or time of the next measurement with the prediction equations,

$$\tilde{\chi}_k^{k-1} = F_k \tilde{\chi}_{k-1}, \quad C_k^{k-1} = F_k C_{k-1} F_k^T + Q_k \quad (36)$$

and the estimated residual becomes,

$$r_k^{k-1} = m_k - H_k \tilde{\chi}_k^{k-1}, \quad R_k^{k-1} = V_k + H_k C_k^{k-1} H_k^T \quad (37)$$

Here  $Q_k$  denotes the additional error introduced by process noise, such as random perturbations of the particle trajectory, for example multiple scattering. The updating of the system state vector with the  $k^{\text{th}}$  measurement is performed with the filter equations,

$$K_k = C_k^{k-1} H_k^T (V_k + H_k C_k^{k-1} H_k^T)^{-1} \quad (38)$$

$$\tilde{\chi}_k = \tilde{\chi}_k^{k-1} + K_k (m_k - H_k \tilde{\chi}_k^{k-1})$$

$$C_k = (1 - K_k H_k) C_k^{k-1}$$

with the filtered residuals

$$r_k = (1 - H_k K_k) r_k^{k-1} \quad R_k = (1 - H_k K_k) V_k \quad (39)$$

$K_k$  is sometimes called the gain matrix. The  $\chi^2$  contribution of the filtered point is then given by

$$\chi_{k,F}^2 = r_k^T R_k^{-1} r_k \quad (40)$$

The system state vector at the last filtered point always contains the full information from all points. If one needs the full state vector at every point of the trajectory, the new information has to be passed upstream with the smoother equations,

$$A_k = C_k F_{k+1}^T (C_{k+1}^k)^{-1}$$

(41)

$$\tilde{x}_k^n = \tilde{x}_k + A_k (\tilde{x}_{k+1}^n - \tilde{x}_{k+1}^k)$$

$$C_k^n = C_k + A_k (C_{k+1}^n - C_{k+1}^k) A_k^T$$

$$r_k^n = m_k - H_k \tilde{x}_k^n$$

$$R_k^n = R_k - H_k A_k (C_{k+1}^n - C_{k+1}^k) A_k^T H_k^T$$

Thus, smoothing is also a recursive operation which proceeds step by step in the direction opposite to that of the filter. The quantities used in each step have been calculated in the preceding filter process. If process noise is taken into account, for example to model multiple scattering, the smoothed trajectory may in general contain small kinks and thus reproduce more closely the real path of the particle.

In the equation above, F and H are just ordinary matrices if both transport and projection in measurement space are linear operations. In the case of non-

linear systems, they have to be replaced by the corresponding functions and their derivatives,

$$F_k \tilde{x}_k \rightarrow f_k(\tilde{x}_k) \qquad H_k \tilde{x}_k \rightarrow h_k(\tilde{x}_k) \qquad (42)$$

using for covariance matrix transformations

$$F_k \rightarrow \frac{\partial f_k}{\partial \tilde{x}_k} \qquad H_k \rightarrow \frac{\partial h_k}{\partial \tilde{x}_k} \qquad (43)$$

The dependence of  $f_k$  and  $h_k$  on the state vector estimate will in general require iteration until the trajectory converges such that all derivatives are calculated at their proper positions.

### 4.3 Typical tracking devices

#### 4.3.1 Single-coordinate measurement

When a particle traverses tracking devices leaving a single coordinate at specific location, the mechanism of measurement will be different depending on the tracking component. As for tracks nearer to the interaction point, in particular solid-state detector such as vertex detectors and micro-vertex detector, the device used is similar to the strip detector concept which using semiconductor-based strips as a widespread type of tracking device. Meanwhile for tracks which slightly far from the central point, sense wires are chosen to detect the track signal within the gaseous chamber.

#### **4.3.1.1 Silicon Strip detector**

The silicon strip detector is a semiconductor-based device structured in strips with widths about 25  $\mu\text{m}$  each. Smaller width can give better precision of the particle trajectories, for instance micro-vertex detector strips are with widths down to 10  $\mu\text{m}$ . Each strip is functioning like a small diode, allowing voltage to get through such that the border between the strips is depleted eventually producing a high resistance volume. When a charged particle traverses the strip plane, pairs of electrons and corresponding holes will be created, which will then be isolated by the voltage and registered as a pulse. The pulse height can be measured by a suitable clustering algorithm, for example centre-of-gravity based, and determines the location passed by the traversing particle. Solid-state detectors are presently the tracking devices with the highest spatial resolution which improve the reconstruction of primary and secondary vertices. Moreover, they are very good to protect against radiation damage. Despite these advantages, solid-state detectors are still unaffordable to be implemented for whole detector volumes as they are presently very expensive.

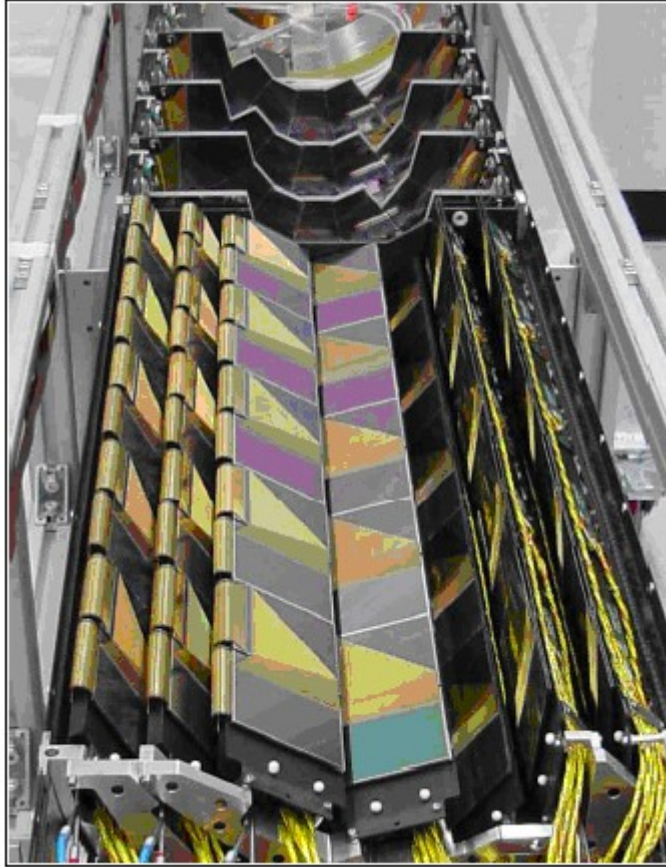


**Figure 4.3** : Lower half barrel of the ZEUS micro-vertex detector

#### **4.3.1.2 Drift chambers**

With significantly large areas to be covered, the gaseous or drift chamber is the most suitable tracking device. To determine the momentum of the traversing particle, the particle needs to move within a magnetic field, and the particle tracks will subsequently provide the leverage that determines the precision of momentum reconstruction. As to that reason, the drift chamber maintains as the largest component in tracking volume.

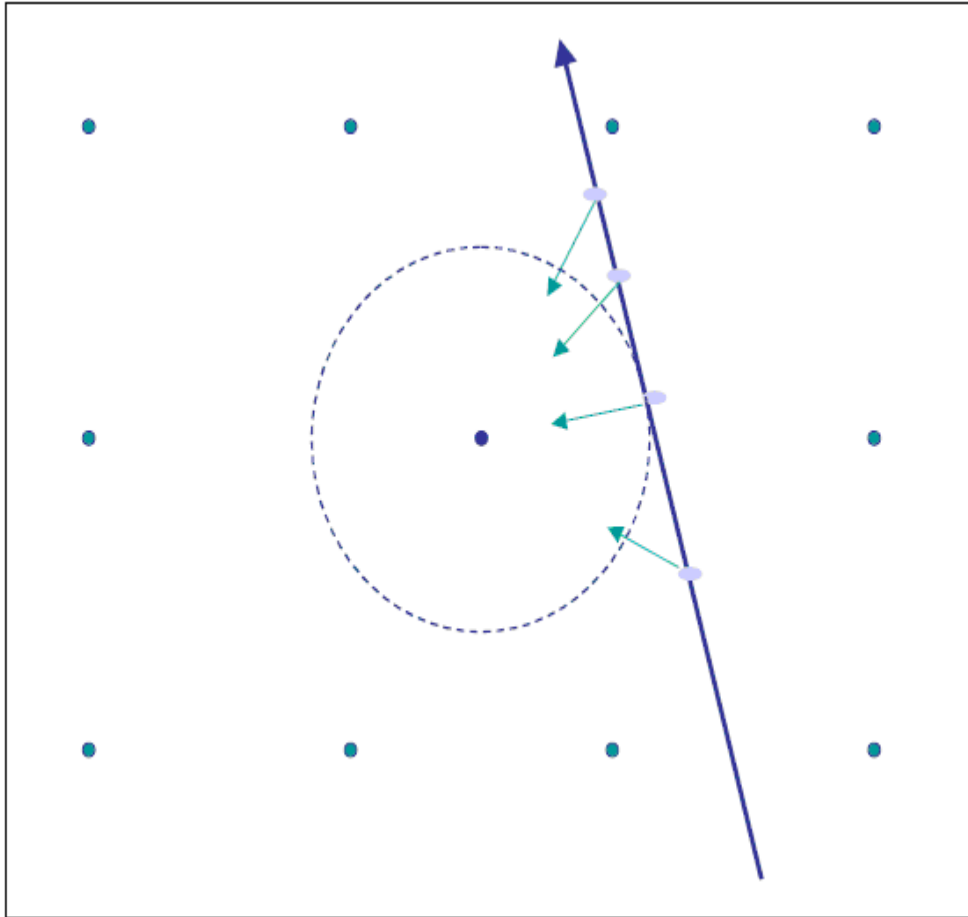
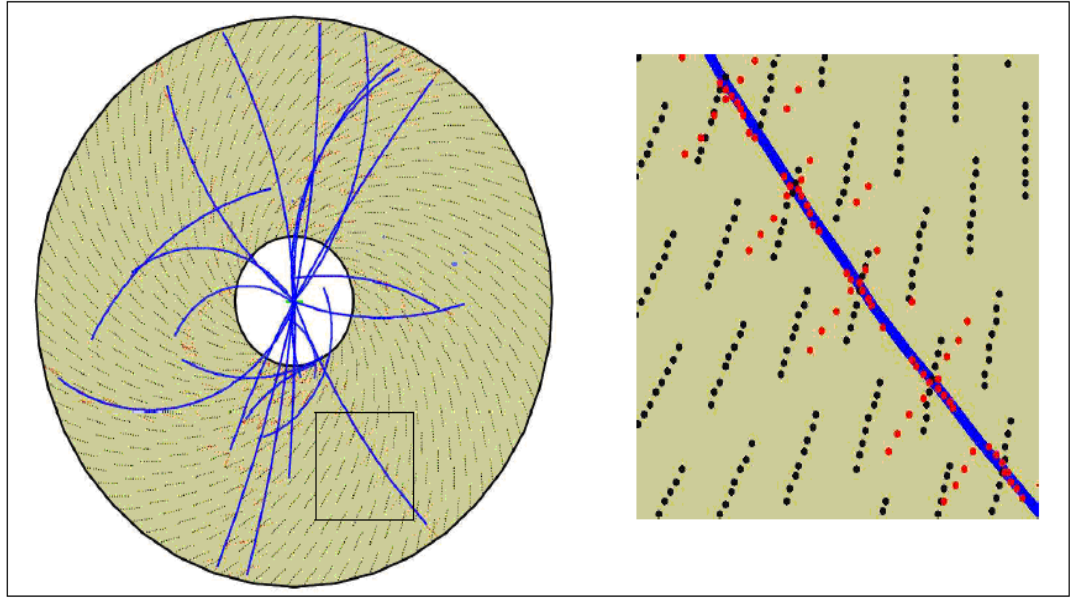


**Figure 4.4:** Schematic view of a drift chamber cell. The closed circle indicates wires, with sense wires in the middle and field wires on the outside. The long and thick arrow represents a trajectory of a particle while the small arrows denote primary ionization charges drifting towards the sense wire.

A drift cell consists of a sense wire or in particular an anode wire in the middle and is surrounded by field wires at the edge. The cell shape is not necessarily rectangular, but adjustable to any other convenient design. Primary ionization occurs along the particle trajectories leaving free charges which subsequently drift to the nearest sense wire. A large number of particles near the sense wire will result a multiplication of ionization which is called gas amplification within a large electric field. The rising edges of signal pick up by the anode wire triggers a time-to-digital converter (TDC) which then measures the

time until a common stop signal. Then, the system will measure the drift time of those charges which are considered as the first to arrive. Generally, in the case of there being more than one particle trajectory at a time in a same drift cell, only the nearest track to the wire will be registered. Also, the single measurement is unable to distinguish which side the particle traverses, resulting in an uncertainty called the left-right ambiguity. Moreover, in the worst case, the left-right ambiguity will produce a mirror track which cannot be distinguished from the real one. However, presently there are better designs developed to overcome this problem.

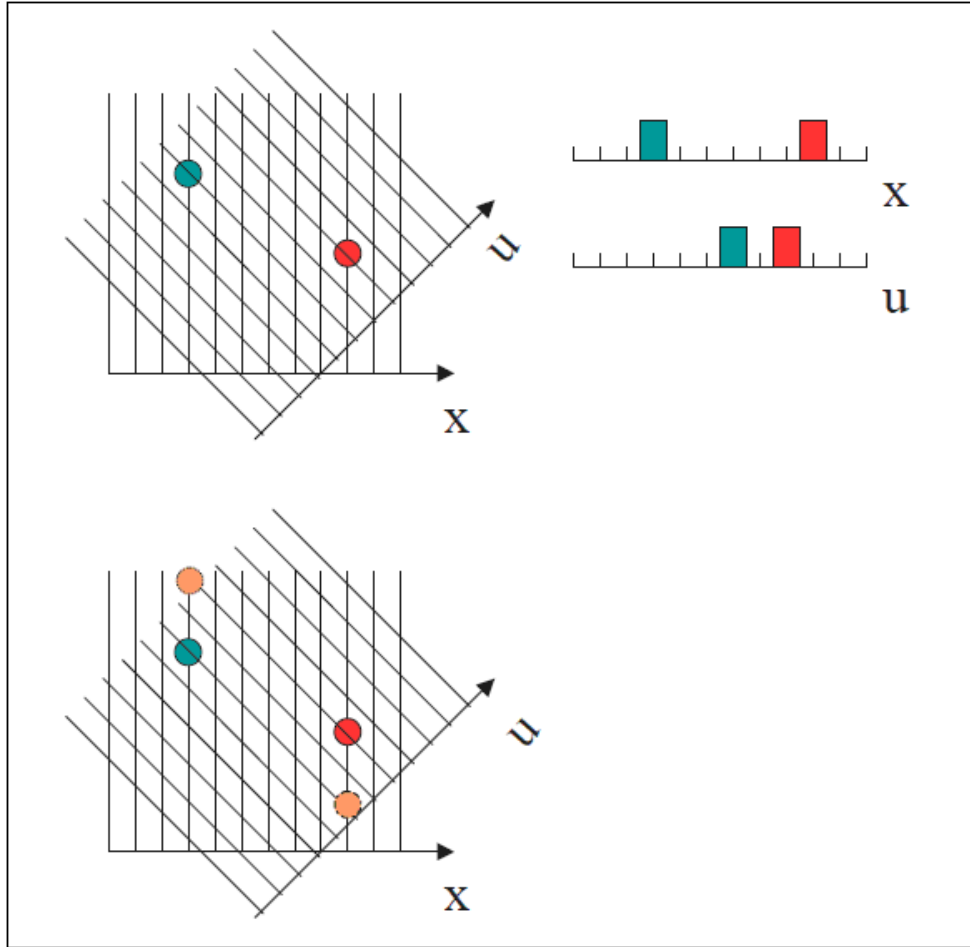
Drift in gases is influenced also by magnetic field. The deviation of the gas drift direction from the vector of the electric field is described by the Lorentz angle. Figure 4.5 shows an event display of the central tracking detector (CTD) of the ZEUS experiment, in the view along the beam axis. The view was taken using a graphic software tool in the ROOT event display. The Lorentz angle in this example is  $45^\circ$  and it is reflected in the design of the cell structure.



**Figure 4.5:** Event display from the ZEUS central tracking detector where the closeup view is given in the square. The blue line is the trajectory and the red dot is the drift distance end points on both side of the corresponding wire.

### 4.3.2 Stereo angle

Single-coordinate measurement is only limited for single trajectory within a projected space but not providing any 3-Dimensional views. Hence, to create a three axial views, several projected space need to be combined, which typically known as stereo views. In several cases which more than one track involved, ambiguities may occur to locate the exact intersection points of the particles where the real points will be seen having a pair. These pairs which commonly recognized as ghost points will create ambiguities in the measurement.



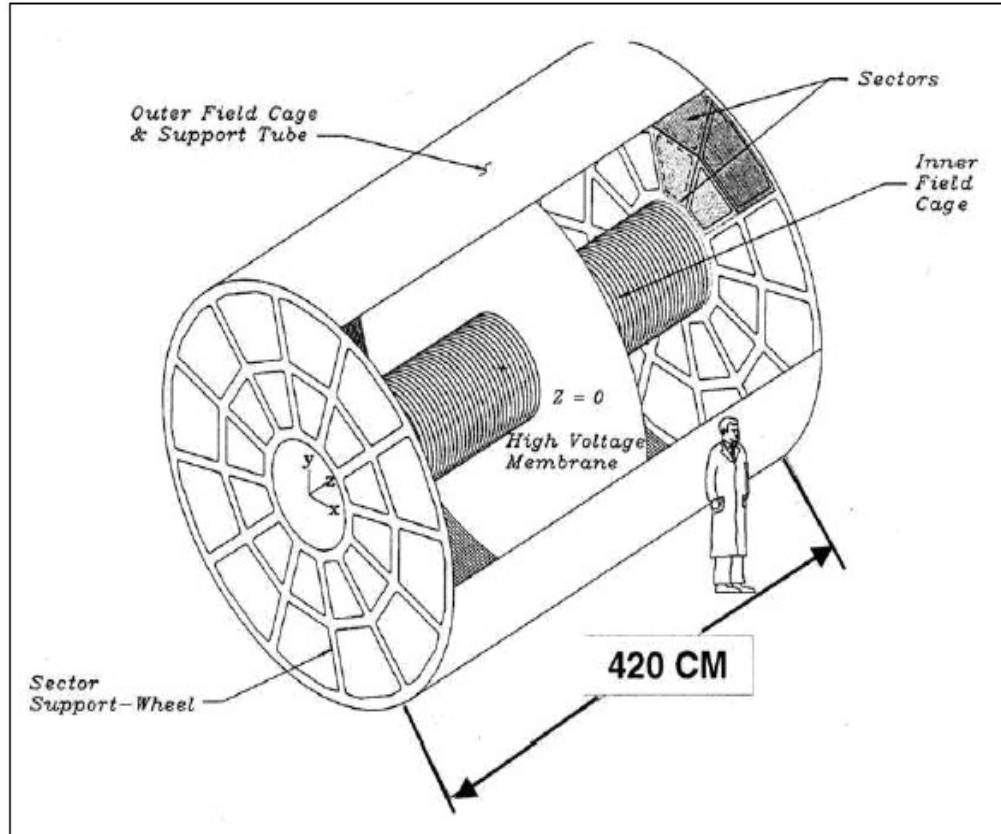
**Figure 4.6** : Top left : The real hit points with two stereo views on x plane ( $0^\circ$ ) and u plane ( $45^\circ$ ). Top right : Single view on x and u plane with two ghost points in blue. Bottom left : Ambiguity hits observed on x and u plane.

Figure 4.6 shows two particle intersection on two strip detector x and u. In this case, since the true tracks are well separated, the uppermost ghost combination is already just outside the chamber acceptance of the u view. This concept is called an all-stereo design. Ambiguities of the assignment of the measured hits in the x and u views to each other lead to the reconstruction of two ghost points. In general at least three views are necessary to avoid this kind of ambiguities. Usage of more than one measurement concepts in detector design, in

general are currently implemented to maximise particle detection capabilities of the detector as well as due to economic reasons.

### **4.3.3 Three-Dimensional (3D) measurement**

Better precision measurement and higher efficiency in avoiding ghost points are the main advantage of using 3-dimensional views. Not only for solid-state detector, 3-dimensional measurement can also be applied to gaseous detector, where the examples can be observed in CCD-based vertex detector in SLD experiment and the TPC in STAR experiment [38]. In 3D views for gaseous chamber, no wires are used, but an electrode membrane is located at the middle plane in axial electric field to drift charges to the anode and be registered.



**Figure 4.7 :** TPC of the STAR experiment.

## 4.4 Performance Evaluation

### 4.4.1 The reference set

Tracks are normally provided by a Monte Carlo simulation and the selection of reference tracks usually depends on the physics motivation of the experiment. However, tracks are disregarded and excluded due to the following reasons,

- Low momentum particles arising from secondary interactions in the material
- Particles traveling outside the geometrical acceptance, for example trajectories within the beam hole of a collider experiment cannot be traced by the detector
- Particles straddling the border of a detector and traversing only a small number of tracking layers. To be regarded as constituents of reference set, particles need to traverse at least 80% of the nominal tracking layers.

The definition of the reference set can be referred as a definition of effective geometrical acceptance

$$\epsilon_{geo} = \frac{N_{ref}}{N_{total}} \quad (44)$$

with  $N_{ref}$  and  $N_{total}$  denoting the numbers of particles of interest in the reference set and in total, respectively.

#### 4.4.2 Track finding efficiency

To evaluate whether a track has been effectively identified or found by the algorithm or not, two different concepts are typically used as benchmarks. Tracks are observed by,

- Hit matching. By using the Monte Carlo truth information, this method analyzes the simulated origin of each reconstructed hit in the reconstructed track. If the qualified majority of hits are at least 70% originates from the same true particle, the track is said to reconstruct this particle. This method is stable in the limit of very high track densities, but requires the Monte Carlo truth information to be mapped meticulously through the whole simulation.
- Parameter Matching. The reconstructed parameters of a track are compared with the true particles. Although this method requires less functionality from the simulated chain, it bears the danger of accepting random coincidence between true particles and artifacts from pattern recognition algorithm.

The reconstruction efficiency can be defined as,

$$\epsilon_{reco} = \frac{N_{ref}^{reco}}{N_{ref}} \quad (45)$$

where  $N_{ref}^{reco}$  is the number of reference particles that are reconstructed by at least one track. Otherwise for the abundance of non-reference tracks which are reconstructed,  $N_{non-ref}^{reco}$  the relation is,

$$\frac{N_{non-ref}^{reco}}{N_{total} - N_{ref}} \ll \epsilon_{reco} \quad (46)$$

#### 4.4.3 Ghosts

Ghosts are defined as the tracks produced by pattern recognition algorithm which does not reconstruct any true particles within or without the reference set.

A ghost rate can be calculated by,

$$\epsilon_{ghost} = \frac{N_{ghost}}{N_{ref}} \quad (47)$$

where  $N_{ghost}$  is the number of ghosts.

The mean number of ghosts per event can also be specified since the ghost rate may be dominated by a small subset of events with copious hit multiplicity.

#### 4.4.4 Clones

‘Clones’ is another term we use to analyze redundant reconstruction of particles. The number of clone can be determined by,

$$N_m^{clone} = N_m^{reco} - 1 \quad \text{if } N_m^{reco} > 0 \quad (48)$$

and otherwise,

$$N_m^{clone} = 0 \quad (49)$$

where  $m$  is the given particle and  $N_m^{reco}$  is its number of reconstructed tracks for  $m$ .

Hence, the clone rate is

$$\epsilon_{clone} = \frac{\sum_m N_m^{clone}}{N_{ref}} \quad (50)$$

#### 4.4.5 Parameter resolution

Physics performance in an experiment is extremely dependent on the quality of reconstructed particle parameters and error estimates from the reconstruction in the detector components. Thus the parameter residual of a track parameter  $X_i$  can be defined as

$$R(X_i) = X_i^{rec} - X_i^{true} \quad (51)$$

where  $X_i^{rec}$  and  $X_i^{true}$  are the reconstructed and true track parameter respectively.

Form equation above, the parameter estimate bias  $\langle R(X_i) \rangle$ , can be obtained. By

using the estimate of the parameter covariance matrix,  $C_{ii}$ , the normalized parameter residual can be defined as

$$P(X_i) = \frac{X_i^{rec} - X_i^{true}}{\sqrt{C_{ii}}} \quad (52)$$